Experimental Results in Nonlinear Compensation of a One Degree-of-Freedom Magnetic Suspension

David L. Trumper, James C. Sanders, Tiep H. Nguyen, and Michael A. Queen
Dept. of Electrical Engineering
Univ. of N. Carolina at Charlotte
Charlotte, NC 28223

1 Introduction

Nonlinear control techniques are of increasing interest in magnetic bearing applications. A one-degree-of-freedom magnetic suspension system has been constructed to serve as a test system for nonlinear control. The objective of this effort is to build an accurate model for the nonlinear suspension dynamics and to show the advantages of compensating for these nonlinearities by using a nonlinear controller. The results obtained with a nonlinear controller are experimentally demonstrated as superior to those obtained with a linear controller. Specifically, a controller which contains a force-control block yields transient responses which are largely independent of the operating point air gap.

A block diagram for the suspension system is shown in Figure 1. As shown in the figure, a one inch steel ball is suspended below a 3500-turn solenoid wound on a one inch steel core. The solenoid is driven by a hysteretic switching current drive. The ball position is sensed using a photodiode array illuminated by an array of infrared LEDs. The system is controlled by a PC-based algorithm and data acquisition system. Within the control algorithm, corrections are made for sensor nonlinearities and for the solenoid nonlinear force characteristics.

Theory for feedback linearization is presented in [1–4]. The application of linearization to magnetic suspension systems has been discussed in [5–10]. The results presented herein are an experimental investigation of ideas presented in [10]. Here, feedback linearizing transformations are demonstrated for second-order and third-order models of a one-degree-of-freedom magnetic suspension. Simulated responses are presented, but no experimental results are given. This is due to two shortcomings. First, the optical sensor used in [10] is not sufficiently stable to allow accurate position measurements which are required to linearize the suspension. Second, the force measurement scheme consists of a balance beam which allows only static force measurements. These deficiencies have been rectified in the present effort, allowing the presentation of experimental results verifying the advantages of using nonlinear compensation for magnetic suspensions.

In the following sections the design of the position sensor, switching power amplifier, force measurement fixture, and nonlinear controller are presented, along with experimental results for the power amplifier, force measurements, and suspension dynamics.

2 Position Sensor

The position sensor works by arranging for the suspended ball to cast a shadow on a 16-element linear photodiode array. The array is illuminated by a vertical linear array of four infrared light emitting diodes. In order to reduce interference from external optical sources, the photodiode array is covered by a piece of red plastic taken from a display bezel, and shielded with a closed-ended tube, in which end a slit has been cut of width sufficient to admit the LED illumination but block most other external light.

In initial work, the individual photodiode currents were used to study the uniformity of illumination, but in operation, all sixteen currents are summed together at the virtual ground input of a transresistance amplifier. The vertical spacing of the LEDs was adjusted to achieve the minimum nonuniformity, but a significant amount remains. Because of this, the sensor output is not purely linear with ball position.

This uniformity is measured by making use of a test fixture which is depicted in Figure 2. Here a test ball is glued into an adapter ring which connects it with a piezoelectric load cell which is itself mounted on an adapter ring which is epoxied onto the anvil of a differential thread micrometer. With this fixture, the ball can be vertically translated with a resolution of better than 10 μm. Simultaneously, the force acting on the ball can be measured via the load cell. Because the piezoelectric load cell is very stiff, the combined system has a resonant frequency of about 5 kHz, which allows the load cell output to be interpreted as measuring applied force for all frequencies of interest. Force measurements are described in more detail in Section 4. Here, the test fixture was used to set a known air gap, and thereby calibrate the position sensor. Because the ball enters the beam from below, the test fixture does not interfere with the optical path when performing this calibration.

Measurements of the uncorrected sensor output indicate a deviation from the best-fit straight line of about ± 1 mm. Samples of the measured data are stored in a table in the control computer, and used to linearly interpolate position, in order to remove this deviation. The controller samples the sensor voltage and updates the control law output at a 1 kHz rate. At each sample, the data table is used to interpolate position by using a bisection algorithm. This corrected position is fed to the lead compensation block and thus to the rest of the loop.

Following this correction, the sensor corrected output shows deviations from a best-fit straight line of about ± 0.1 mm. The largest remaining error term is due to instability of the LED intensity, primarily with respect to temperature. This instability limits the accuracy of the data table used for interpolation. In future implementations, it would be advantageous to design a sensor in which absolute intensity is not of first-order importance to the measurement. One approach would be to use a lateral effect photocell, in which the location of the illumination rather than its intensity is the important parameter. In any case, the sensor linearity is satisfactory for the current purposes.

3 Power Amplifier

A schematic for the solenoid current drive is shown in Figure 3. The power amplifier is of the

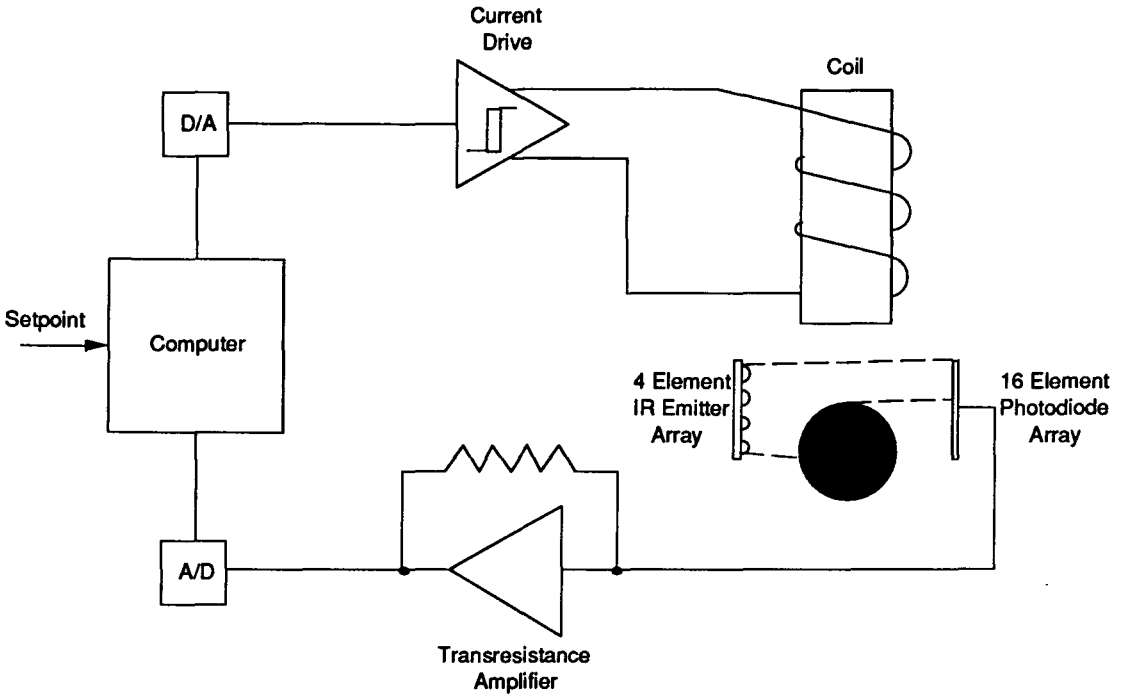

Figure 1: Control loop block diagram.

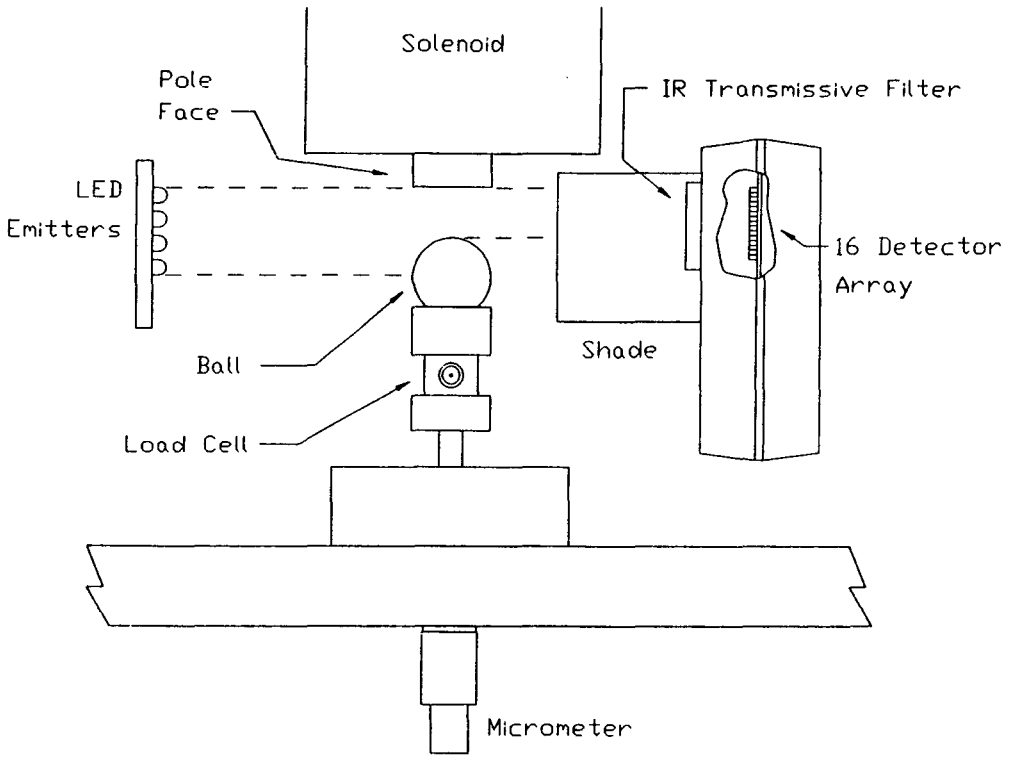

Figure 2: Micrometer and load cell fixture.

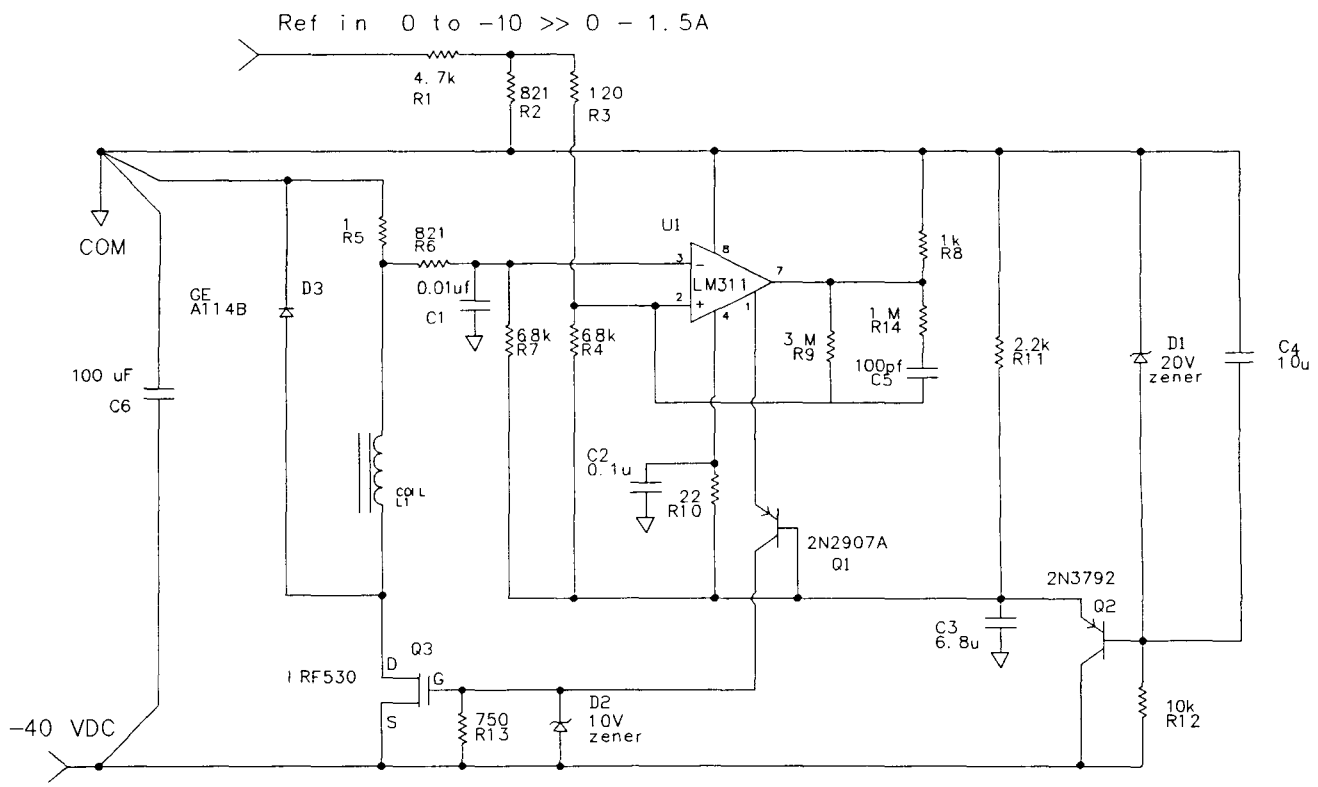

Figure 3: Current drive schematic.

hysteretic type. A comparison of this type of converter to sample/hold and minimum pulse width converters is given in [11]. The operation of the amplifier is described as follows.

The coil voltage is controlled by transistor Q_3 acting as a switch. When Q_3 is on, 40 volts is applied to the coil, thereby increasing the coil current. When Q_3 is off, the coil current freewheels through the flyback diode D_3, thereby decreasing the coil current. The switching of Q_3 is controlled by comparator U_1 through the common base transistor Q_1 which provides level shifting, and the gate-network D_2–R_{13} which limits the gate voltage to 10 volts when Q_1 is on and provides a turn-off path when Q_1 is off.

Comparator U_1 switches on and off based upon the difference between the reference level as scaled by the input network R_1–R_4 and the actual current level as measured by sense resistor R_5. The switching has a hysteretic component determined by the feedback network R_9, R_{14}, and C_5. Components R_{14} and C_5 are included to eliminate a burst of oscillation which occurred on the comparator switching transients and which resulted in undue heating of the power FET Q_3. The R_6-C_1 low pass filter serves to attenuate spikes due to stray inductance in R_5 and feedthrough capacitance in the solenoid coil L_1. Without this filter, the supply oscillates at about 1 MHz.

A goal of this design is to operate with only a single external power supply. Thus transistor Q_2 and its bias network are used to supply -20 volts to the low side of comparator U_1. Through resistors R_7 and R_4 this -20 volt supply is used to offset the comparator input voltages to within the allowable common mode range of the comparator. Resistors R_7 and R_4 are adjusted relative to the values in the rest of the input network in order to reject changes in the -20 volt supply level. This prevents transients on the -20 volt supply from disturbing the switching thresholds. One additional consequence of the chosen topology is that the reference voltage must go negative to set an increase in the coil current.

The solenoid consists of 3500 turns of #22 wire, with a room temperature resistance of $R_L = 28$ Ohms. This resistance rises to about $R_L = 33$ Ohms at the typical operating temperature ($i_L = 0.6$A). If the solenoid is alternately switched between 0 and 40 Volts, the resulting current waveform has an exponential time constant of about 60 msec, implying a low-frequency coil inductance of about 2 H. However, based upon measurements at the 10 kHz supply mid-point operating frequency, the coil demonstrates a high-frequency incremental inductance of 200 mH. This value is used in the analysis which follows.

In operation, the coil current will oscillate between a low-threshold current I_1 and high-threshold current I_2. This oscillation will take the form of an asymmetric triangle wave, with I_1 and I_2 set by the reference voltage and the amount of comparator hysteresis. Neglecting the flyback diode voltage drop, the cycle time T for this oscillation is given by

$$T = -\tau \ln\left(\frac{I_1(I_F - I_2)}{I_2(I_F - I_1)}\right) \tag{1}$$

where $\tau = L_1/(R_5 + R_L)$, and $I_F = 40/(R_5 + R_L)$ is the full scale current which results if the switch Q_1 remains closed. For the design values,

$$I_1 = -0.1488 V_{ref} - 5.605 \times 10^{-3} \tag{2}$$

and

$$I_2 = -0.1488 V_{ref} - 9.766 \times 10^{-4} \tag{3}$$

There is thus $I_2 - I_1 \approx 4.6$ mA of switching ripple, and the current remains within about 2.3 mA of the setpoint for all inputs which do not exceed the current slew rate limit imposed by the finite supply voltages. This latter limitation has a significant impact on closed-loop operation as discussed in Section 5.

The switching frequency is given by $1/T$. Using the results from (1)–(3), the switching frequency as a function of average current $(I_1 + I_2)/2$ is calculated and compared to the measured frequency in Figure 4. Note that the frequency is zero at both zero and full-scale currents, and peaks at about the mid-scale current. The measured frequency was recorded as the current was increased from zero to full scale, and closely matches the calculated frequency. However the actual frequency exhibits significant hysteresis dependent upon the time history of supply current. This effect is due to the magnetic hysteresis in the solenoid core, and can be as large as 2 kHz at the maximum frequency point.

4 Force Measurements

The electromagnet force as a function of position and current is measured with the load cell and micrometer fixture which was used to calibrate the optical sensor. With the micrometer at a fixed position, the electromagnet current is cycled from zero to full scale and then back to zero, with a triangular time dependence. Over multiple cycles, the load cell amplifier output is measured at about 200 points within each cycle and averaged at each point over the multiple cycles. The form of the resulting data is shown in Figure 5.

The force curves exhibit significant hysteresis, which is due to using cold-rolled steel as the core material. In future designs, a magnetically-softer material should be used. Also note that the hysteresis curves have essentially constant width in current, independent of air gap. This is explained by the fact that the ball is only weakly coupled to the core and thus the core flux is largely independent of ball position.

The measured force rises as the square of current for low currents, as would be predicted by a first order field analysis, and then rises less strongly at higher currents, due to saturation in the core. In the low-current region ($i < 0.4$A), the force is well modeled by

$$F = C \left(\frac{i}{x + 0.0025} \right)^2 \tag{4}$$

where F is the electromagnet force in Newtons, i is the coil current in amps, x is the air gap in meters, and $C = 6.5 \times 10^{-4}$ Nm^2/A^2. Note that the actual air gap plus 2.5 mm is used in this law. This accounts for the fact that the force does not become infinite at zero air gap. Beyond 0.4 Amps, saturation becomes significant, and a more complex model is required.

The force curves exhibit significant hysteresis, which is due to using cold-rolled steel as the core material. In future designs, a magnetically-softer material should be used. Also note that the hysteresis curves have essentially constant width in current, independent of air gap.

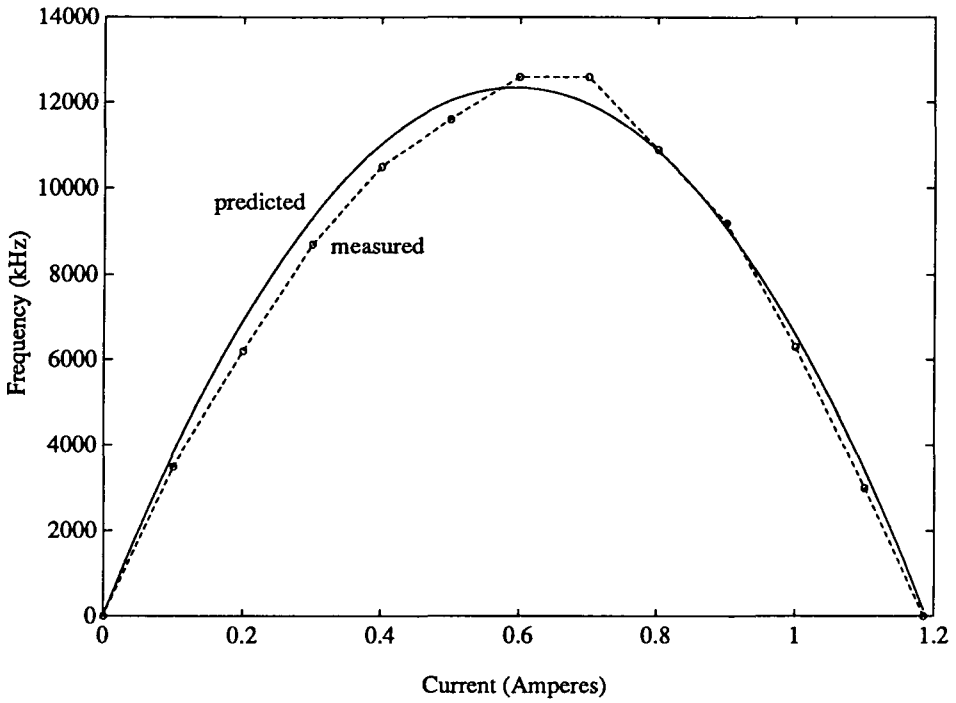

Figure 4: Switching frequency as a function of current.

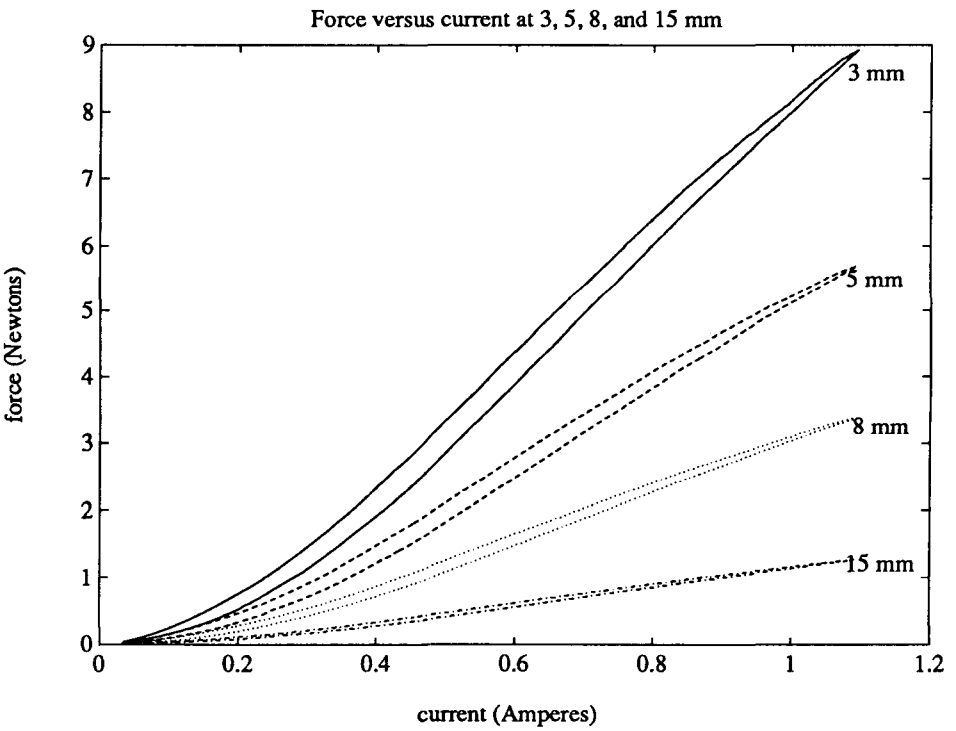

Figure 5: Uncompensated electromagnet force as a function of current at air gaps of 3, 5, 8, and 15 mm.

This is explained by the fact that the ball is only weakly coupled to the core and thus the core flux is largely independent of ball position.

However, this model is not developed in the i-F plane, since for the present purpose of nonlinear compensation what is required is a function which, given the air gap x and a desired force F_d, yields the current in Amperes necessary to realize this force. At low forces relative to the air gap, this function is found by inverting (4), and thus increases linearly with air gap and as the square root of desired force. At higher forces, the current must grow more strongly with desired force. A reasonable fit to the data has been empirically found to be

$$i_s = (x + 0.0025)\sqrt{\frac{F_d}{C}} + \left(0.0195e^{\left(\frac{x-0.002}{0.006}\right)} - 2.5(x - 0.01)\right) F_d + 400(x - 0.002)^2 F_d^2 \quad (5)$$

This function fits the data well over the operating range of the suspension.

The quality of the fit achieved by (5) is determined experimentally by writing a test program which cyclically ramps the desired force up and down while measuring the actual force with the load cell fixture. The results of this experiment are shown in Figure 6. The four traces shown in the figure are for air gaps of 3, 5, 8, and 15 mm; these traces essentially overlay, showing the success of the compensation (5). There is however, an error of about 10% in the gain, and the force drops off slightly from a straight line at high current and the smaller air gaps. The source of the gain error has not yet been adequately identified, as the data has only recently been acquired. However, hysteresis represents the most significant error term, particularly at small air gaps, where the force hysteresis magnitude approaches the weight of the ball. As mentioned above, this error term can best be addressed by using a magnetically-softer core material.

The results of the above force modeling are used to design the nonlinear compensator, which is described in the next section.

5 Nonlinear vs. Linear Control

A block diagram for the nonlinear compensation control loop is shown in Figure 7. The blocks labelled Sensor Compensator, Lead Compensator, Gain, and Nonlinear Compensator are implemented in floating point arithmetic within the control computer, which is an 80386/80387-based system with a processor clock frequency of 20 MHz. The A/D and D/A converters both have 12-bit resolution, and reside on a circuit card within the computer. The current drive, electromagnet, and sensor have been described in detail above. The mass of the ball $M = 0.06$ kg times the acceleration of gravity g is equal to approximately 0.6 Newtons. This force sums with the electromagnet force as the input to the block labelled $1/Ms^2$ which has air gap x as its output.

All the blocks within the control computer algorithm are updated at a 1 kHz rate. The Nonlinear Compensation block implements (5) appropriately scaled for the 12-bit D/A converter, and for the algorithm air gap representation in millimeters. The anticipated gravity load of 0.6 N is added to the error signal to give $F_d = F_e + 0.6$ which is input to the Nonlinear Compensation block as the force to be maintained on the ball. Adding the gravity load at this

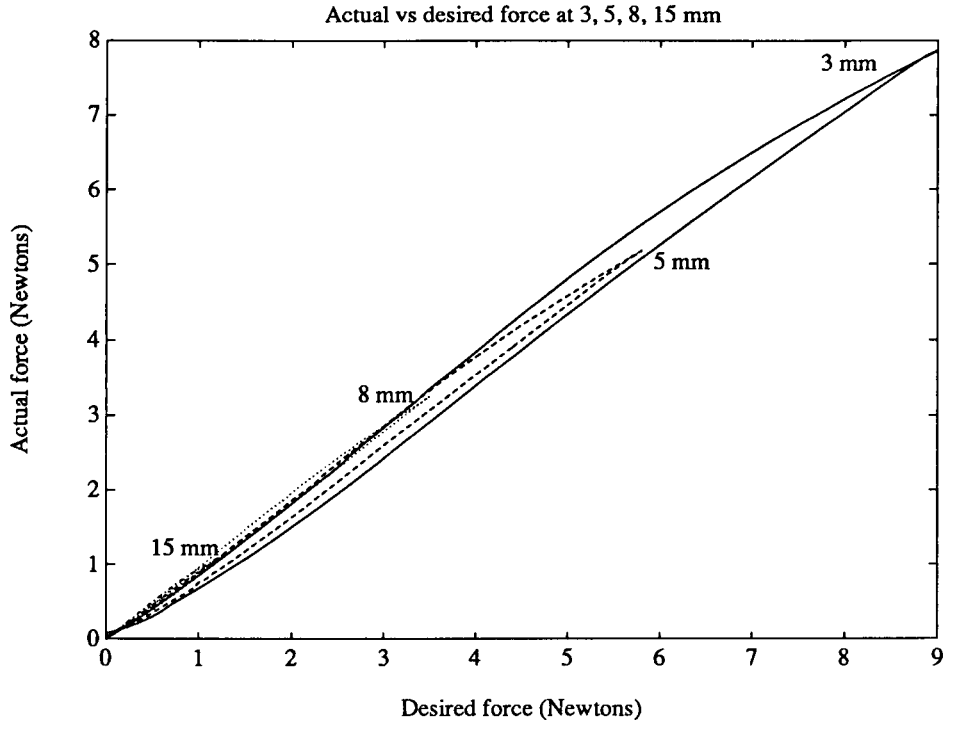

Figure 6: Compensated electromagnet force as a function of desired force at air gaps of 3, 5, 8, and 15 mm.

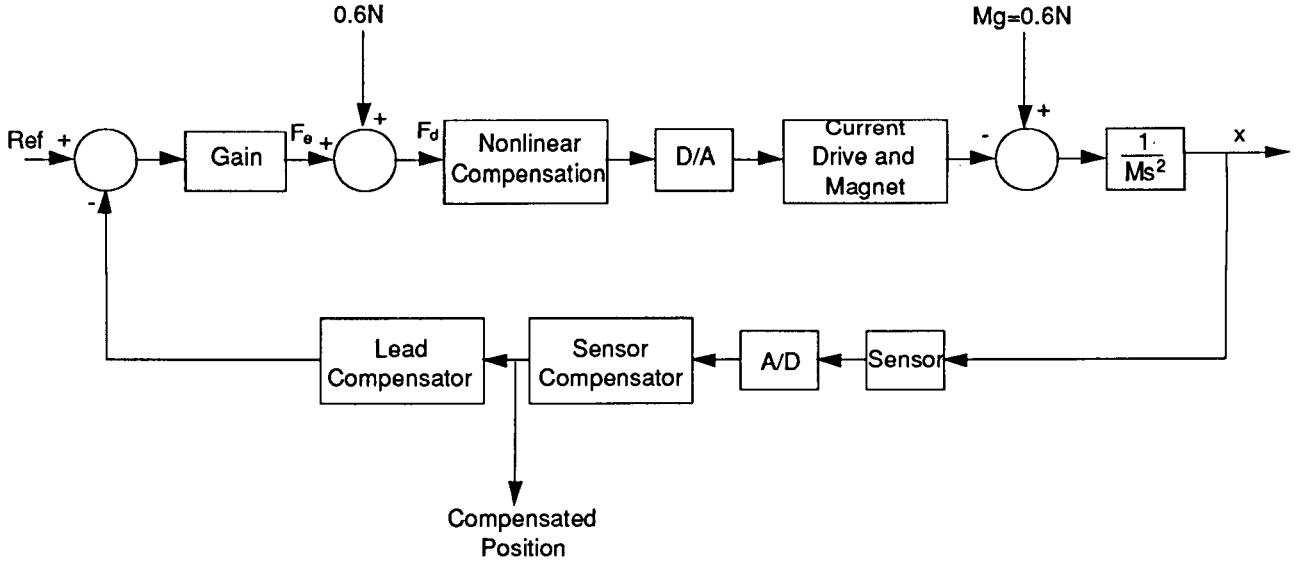

Figure 7: Nonlinear compensated control loop block diagram.

point greatly reduces the static error in suspension, since the loop uses only lead compensation and thus is of type 0. The reference signal is subtracted from the output of the lead compensator to yield the force error F_e. The loop lead compensation is placed in the feedback path in order to reduce the amplitude of the transient under step inputs as compared with placing the lead compensator in the forward path. The lead compensator has a zero at $z = 0.94$, a pole at $z = 0$, and a DC gain of unity.

The linear loop uses the same lead compensation singularity locations, but differs from the nonlinear loop in that the nonlinear compensation operation is replaced by a constant gain. Additionally, it is not possible to add a constant force offset term in the linear case. The error under Type 0 linear compensation has been found to reach 4–5 mm at the largest air gaps. Thus, in the linear compensation, the reference input is manually reset to achieve a desired air gap. All results are reported herein in terms of actual air gap.

A comparison of the loop performance under linear and nonlinear compensation is made as follows. At an air gap of 14.6 mm, both the linear and nonlinear compensator gains are adjusted to achieve essentially identical step responses with approximately 26 msec rise time. Then these gains are left unchanged as the air gap is set to 8.4 mm, 5.7 mm, and 3.7 mm. The resulting transients for the nonlinear and linear compensated systems are shown in Figure 8. In each of the figures, the top trace represents the compensated air gap as output by the Sensor Compensation block, with a sensitivity of 0.1 mm per division. Thus the steps shown represent a change in position of approximately 0.25 mm. The lower trace in each figure is the coil current as measured by a hall effect probe. This trace is AC coupled, and has a sensitivity of 50 mA per division.

As shown in the figures, the nonlinear compensated loop maintains a nearly constant step response as the air gap is reduced by about a factor of four, whereas the linear compensated loop performance deteriorates significantly. One measure of this change is the asymmetry between the positive going and negative going transients. Since the top trace represents the air gap which increases as the ball moves away from the pole face, the positive-going transient is associated with the ball moving away from the pole face, and likewise the negative-going transient is associated with the ball moving toward the pole face.

Another measure is the variation in rise and fall times as indicated on each trace. The rise and fall times for the nonlinear compensation loop remain symmetric at approximately 25 msec for all responses except at 3.7 mm where a small amount of asymmetry is visible, and the rise time increases slightly to about 29 msec. By comparison, the rise and fall times for the linear compensation loop change dramatically and exhibit significant asymmetry, as shown in the figure. The associated current traces also show significant asymmetry under the linear compensator, but remain symmetric under the nonlinear compensator. Note that as the air gap is reduced, the magnitude of the current transient decreases, since the incremental current-to-force gain of the electromagnet increases at smaller air gaps.

The transients shown in Figure 8 are the result of averaging 32 traces. This was done to eliminate a baseline limit-cycle noise of approximately 50 mV. The magnitude and dominant frequency of this noise depend strongly upon the controller gain, lead-zero location, and operating point air gap. The cause of this limit cycle has not yet been thoroughly

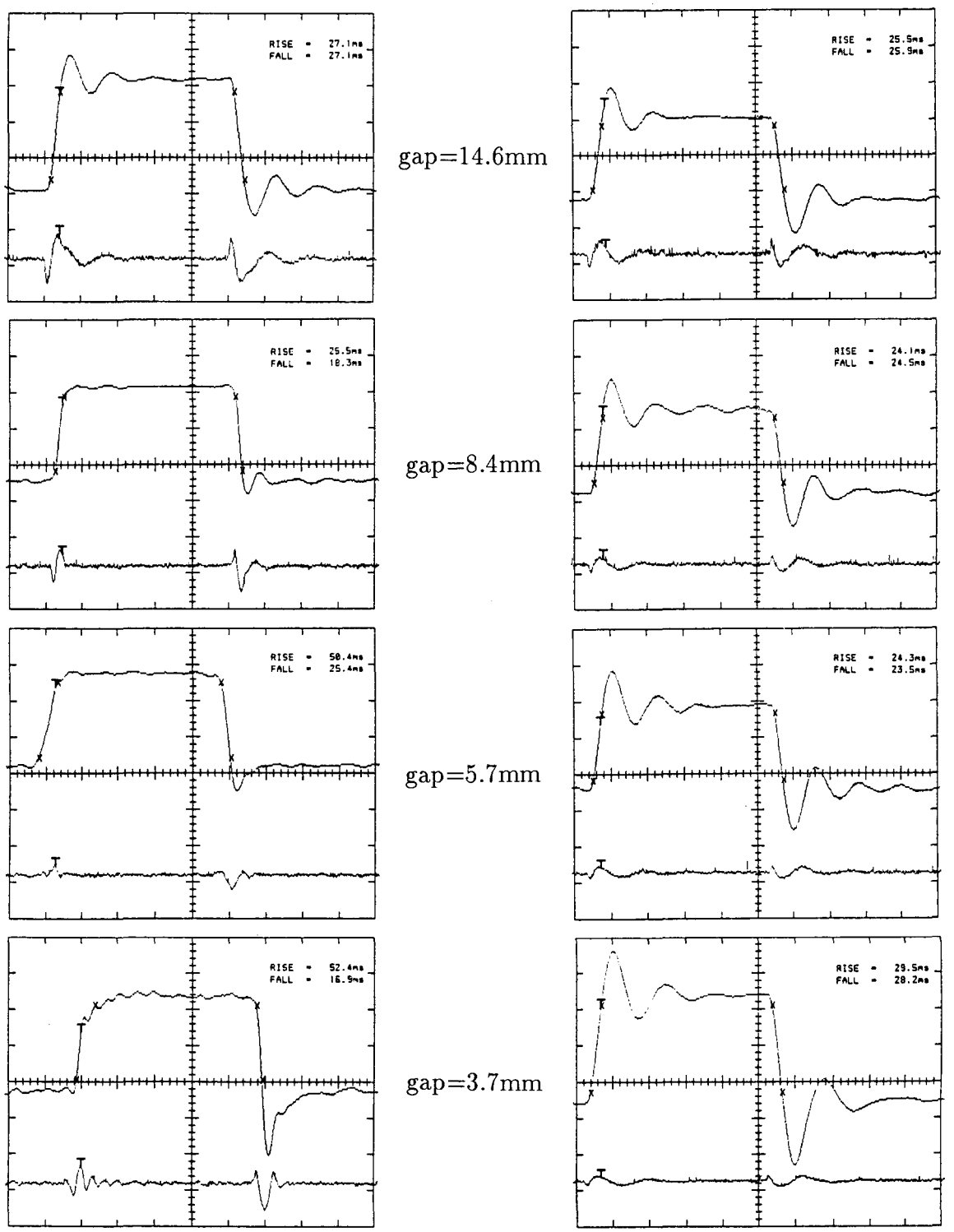

Figure 8: Step responses of linear and nonlinear compensated loops at air gaps of 14.6, 8.4, 5.7, and 3.7 mm (top to bottom). Left column shows response with linear compensator. Right column shows response with nonlinear compensator. In both columns, the top trace is incremental air gap, 0.1 mm/div, and the bottom trace is coil current, 50 mA/div. The time base is 100 msec/div for all traces.

investigated; however it is believed to be due to the finite quantization levels of the 12-bit converter used in these experiments. This is physically reasonable, since for the ± 10 volt range of the converter, the least significant bit represents about 5 mV, and thus the limit cycle entails a total span of about 10 least significant bits. For an open-loop unstable system such as this suspension, some amount of limit cycling is inevitable in the presence of amplitude quantization. A describing-function analysis of the quantized loop and simulation experiments are planned to verify quantization as the cause of this behavior.

Another destabilizing effect, which can be observed if the current trace is examined in detail, is voltage saturation of the current drive. The current drive operates from a unipolar 40 volt supply. Thus, especially at small air gaps when the current required for suspension is small, the maximum negative slew rate is highly constrained. This slew rate limiting becomes significant when the ball is stepped towards the pole face. Initially, current is increased to draw the ball toward the pole face, but then must be rapidly decreased to stop the ball at its new closer position. If the current cannot be rapidly decreased, the ball strongly overshoots. This effect contributes significantly to the asymmetric transients observed for the linear compensator in Figure 8, and also can degrade the stability of the nonlinear compensated loop if the gain is increased much above the value used in Figure 8. In the describing function sense, the lagging current which occurs in saturation adds negative phase shift which degrades the loop stability.

At small air gaps, the current source voltage saturation can lead to loss of control as shown in Figure 9. Here, the linearly compensated system is operating at a gain higher than that shown in Figure 8, but still within the short-term stability boundary. However, once every few minutes, stability is lost. The trace shown in this figure captures that process. The transient is negative-going, and thus toward the pole face. As the transient is initiated, the current is increased to draw the ball upward, and then enters voltage saturation in which the current source power FET is shut off for approximately 30 msec, during which time the trace takes the form of a decaying exponential, since the coil voltage is constant and equal to zero minus the flyback diode voltage drop. In the second and later transients, the current actually does reach zero. By this process, the ball diverges from suspension.

To avoid this effect, it is clear that the current source must be modified to be capable of applying bipolar voltages to the coil. This can be accomplished within the framework of the present hysteretic design by replacing the single power FET with an H-bridge driver. These are available from a number of manufacturers in integrated form.

6 Conclusions and suggestions for further work

The experimental results presented herein demonstrate the effectiveness of using nonlinear compensation for variable reluctance magnetic suspensions. Several improvements are suggested within the text. The most significant of these is to adopt a current source which has a bipolar voltage capability, so as to avoid the current slew-rate saturation which has been shown to destabilize the loop under certain conditions. The quantization-driven limit cycles which were observed require more investigation; it is likely that a higher-resolution

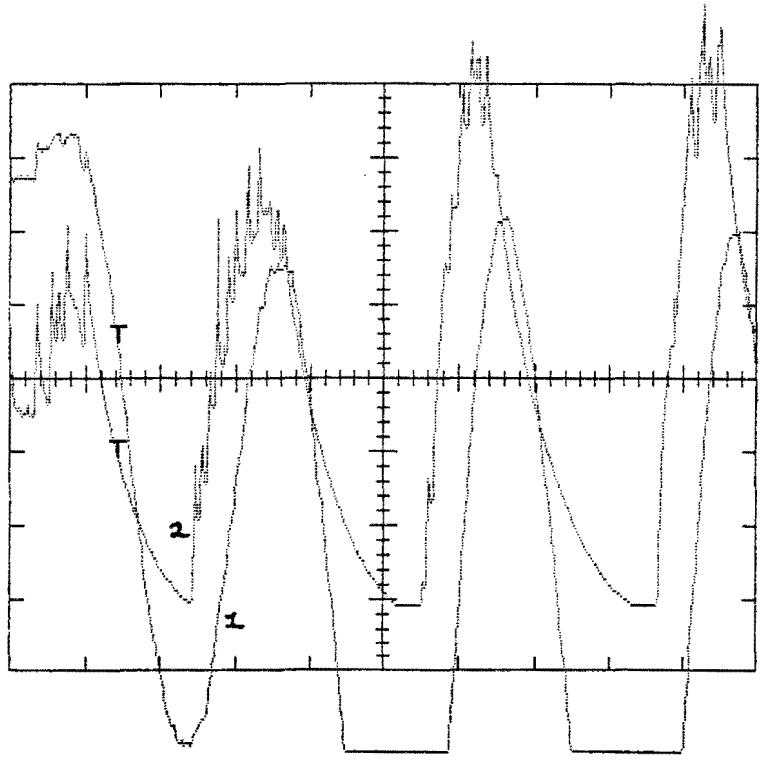

Figure 9: Loss of suspension due to current source voltage saturation. Trace 1 is position at 0.05 mm/div, and trace 2 is current at 20 mA/div. The time base is 20 msec/div.

converter would reduce the magnitude of these cycles. The core should be replaced with a lower-hysteresis material in order to improve the accuracy of the force correction. At very small air gaps (< 1 mm), this remanent magnetization is sufficient to lift the ball, and control is lost. Also, the pole face should made somewhat conical, in order to more strongly center the ball. At very small air gaps, the ball was observed to pull out to the corner of the pole face where the field is more concentrated. Finally, the optical sensor stability could be improved, perhaps by using a lateral effect photo-sensor.

7 References

[1] Slotine, J. E., and Li, W., *Applied Nonlinear Control,* Prentice-Hall, 1991

[2] Spong, M., and Vidyasagar, M., *Robot Dynamics and Control*, Wiley, 1989, pp. 259-283.

[3] Su, R., "On the linear equivalents of nonlinear systems," Systems and Control Letters, vol. 2, No. 1, pp. 48-52, July, 1982.

[4] Hunt, L.R., Su, R., and Meyer, G., "Global Transformations of Nonlinear Systems," IEEE Transactions on Automatic Control, Vol. AC-28, No. 1, Jan., 1983.

[5] Jayawant, B.V., Hodkinson, R.L., Wheeler, A.R., and Whorlow, R.J., "Transducers and Their Influence in the Design of Magnetically Suspended Vehicles," I.E.E. Conf. on Control Aspects of New Forms of Guided Land Transport, I.E.E. Publication No. 117, Aug., 1974, pp. 200–206.

[6] Jayawant, B.V., Sinha, P.K., Wheeler, A.R., and Whorlow, R.J., "Development of 1-ton Magnetically Suspended Vehicle Using Controlled D.C. Electromagnets," *Proc. I.E.E.*, Vol. 123, No. 9, Sept., 1976.

[7] Groom, N.J., and Waldeck, G.C., "Magnetic Suspension System for a Laboratory Model Annular Momentum Control Device," AIAA Paper No. 79-1755, 1979.

[8] Traxler, A., Meyer, F., and Murbach, H., "Fast Digital Control of a Magnetic Bearing with a Microprocessor," International Kongress Mikroelektronik, Munich, Nov 13-15, 1984, pp 94-102.

[9] Trumper, D.L., "Magnetic Suspension Techniques for Precision Motion Control," Ph.D. Thesis, Dept. of Elec. Eng. and Comp. Sci., M.I.T., Camb., Mass., Sept., 1990.

[10] Trumper, D.L., "Nonlinear Compensation Techniques for Magnetic Suspension Systems," NASA Workshop on Aerospace Applications of Magnetic Suspension Technology, Hampton, VA, Sept. 25–27, 1990.

[11] Keith, F. J., et al. , "Switching Amplifier Design for Magnetic Bearings," Proceedings of the Second International Symposium on Magnetic Bearings, Tokyo, Japan, July 12–14, 1990, pp. 211–218.